Static and Dynamical Properties of a Polymer Solution with Upper and Lower Critical Solution Points. NBS 705 Polystyrene in Methyl Acetate

Kenji Kubota, Kathleen M. Abbey, and Ben Chu*

Chemistry Department, State University of New York at Stony Brook, Long Island, New York 11794. *Received March 9, 1982*

ABSTRACT: Laser light scattering has been used to determine the osmotic compressibility, the radius of gyration, the second virial coefficient, the diffusion coefficient, and the frictional coefficient of polystyrene (NBS 705 standard, M_w = 179 000) in methyl acetate from dilute solution to semidilute solution over a range of temperature from 30 to 125 °C. In this system, the upper and lower critical solution temperatures differ by about 125 °C and the Θ temperatures by only about 71 °C. We determined the Θ temperatures to be about 43 and 114 °C. Consequently, we were able to study the static and dynamical properties of a polymer solution from near the upper critical solution temperature (UCST) to near the lower critical solution temperature (LCST). From these data and by analogy with solution properties near the upper critical solution temperature, we present a schematic temperature–concentration diagram for polystyrene in methyl acetate incorporating UCST and LCST as well as the upper and lower Θ temperatures (Θ_U and Θ_L). An interesting observation of the polystyrene–methyl acetate system is that in the reduced temperature–concentration diagram, the NBS 705 standard polystyrene in methyl acetate does not have a really good solvent regime and is dominated by the Θ region covering a very large temperature range due to the finite polymer molecular weight.

Introduction

Recent theoretical advances made by Edwards,[1] de Gennes,[2] des Cloizeaux,[3] and others[4] have provided great insight into the nature and properties of polymer solution behavior from dilute solution to semidilute and concentrated solution regions. Considerable experimental evidence now exists to support the general predictions of the scaling theory using a variety of modern experimental techniques. In particular, small-angle neutron scattering[5–8] (SANS) and laser light scattering[9–11] experiments have been used not only to confirm the scaling laws but also to show deviations in the transition region where the scaling approach is expected to fail. Experiments thus far published have been performed mainly in the region associated with the upper critical solution temperature (UCST), either near the Flory Θ temperature or in the good solvent region above the Θ temperature. A natural extension of the above studies is to investigate the polymer solution behavior in the lower critical solution temperature (LCST) region so that we can cover the temperature–composition diagram from the upper critical solution temperature to the lower critical solution temperature.

Phase diagrams of polymer solutions have been classified into two types of cloud-point curves.[12] The upper critical mixing point (UCP) moves toward lower concentrations and higher temperatures with increasing polymer molecular weight and coincides with the Flory Θ temperature at infinite molecular weight and zero concentration. The identification of the Flory Θ temperature at infinite polymer molecular weight as a tricritical point was proposed by de Gennes.[2] Solutions with finite molecular weight polymers display "ideal" behavior at a second, higher temperature, but lower than the lower critical solution temperature, which is in the neighborhood of the gas–liquid critical temperature of the solvent. Immiscibility occurs if the temperature of the polymer solution is raised above the lower cloud-point (LCP) curve or is lowered below the upper cloud-point curve. The existence of UCST and LCST pairs is a very widespread phenomenon and has been discussed in terms of the thermodynamics of polymer solutions.[13,14] For some polymer–solvent systems, the region of complete miscibility may be quite limited. Only a small number of UCST and LCST pairs for polymer solutions are known.[15] The upper and lower critical solution temperatures for the polystyrene (M_w = 1.8×10^5, M_w/M_n = 1.07)–methyl acetate system differ by only about 125 °C and the Θ temperatures by only about 70 °C. Consequently, we can monitor the change in quality of the solvent over a range of temperatures that are experimentally accessible. Preliminary measurements in the mapping of static and dynamical properties of polystyrene in methyl acetate have been reported.[16,17] There have been some recent results concerning static properties of polystyrene in cyclohexane over a temperature range covering the lower critical solution temperature using SANS.[18] We report here the results of laser light scattering experiments, including the angular dependence of absolute scattered intensity and the Rayleigh line width correlation profile analysis from dilute to semidilute and concentrated solutions over a broad range of temperatures covering the UCST and LCST regions. We are particularly interested in examining the static and dynamical properties of polymer solution near the *lower* Θ temperature because its origin is assumed to differ from the upper Flory Θ temperature.

Experimental Methods

Sample Preparation. Polystyrene (NBS 705 standard, M_w = 179 300, M_w/M_n = 1.07) was dissolved in benzene and then freeze-dried under vacuum. Methyl acetate was dried over P_2O_5 and fractionally distilled twice (over P_2O_5) under a dry nitrogen atmosphere. We first made a 5 wt % solution and then filtered it through a Millipore filter of 0.22-μm nominal pore diameter. Solutions at lower concentrations were prepared by dilution of a known amount of the filtered stock solution directly in the light scattering cell using filtered and purified methyl acetate. Those at higher concentrations were prepared by evaporation of the solvent from a known amount of the filtered stock solution in the light scattering cell using a mild vacuum. All cells containing solutions of desired concentrations were subsequently flame sealed. By the above method of preparation, we were able to cover a concentration range of about 0.3–33 wt %.

Apparatus. The detailed design of the light scattering spectrometer has been described elsewhere.[19,20] We used two spectrometers of similar design, one operating at λ_0 = 632.8 nm, the other at λ_0 = 488.0 nm. The intensity of scattered light was measured mainly using a modified Malvern goniometer with a helium–neon laser. Acquisition of data from the ITT FW130 photomultiplier tube was controlled by a PDP 11/35 minicomputer and scanning was done automatically.[16] Temperature was controlled to 0.01 °C near room temperature and to 0.05 °C at temperatures above 50 °C. The refractive index increment, $(\partial n/\partial C)_{T,N}$, was determined using a Brice Phoenix differential

0024-9297/83/2216-0137$01.50/0

refractometer. Dynamic light scattering measurements were made using both the modified Malvern goniometer with a helium–neon laser and the light scattering spectrometer with an argon ion laser; the latter instrument was the same one used in our studies of polystyrene in *trans*-Decalin.[10]

Data Analysis

Static Properties. Measurements of the angular distribution of the absolute scattered intensity in dilute solution yield

$$\frac{HC^v}{R_c(C^v,K)} = \left(\frac{1}{M_w} + 2A_2C^v\right)\left(1 + (1 + 2A_2C^vM_w)^{-1}\frac{\langle r_g^2(C^v)\rangle_z}{3}K^2\right) \quad (1)$$

where $H = 4\pi^2n^2(\partial n/\partial C^v)_{T,P}^2/(N_A\lambda_0^4)$, with n, C^v, N_A, and λ_0 being the refractive index, the polymer concentration in g/cm^3, the Avogadro number, and the wavelength of light in vacuo, respectively, and K [$=(4\pi/\lambda)\sin(\theta/2)$] is the magnitude of the momentum transfer vector. We can define an apparent radius of gyration at finite concentrations such that

$$\langle r_g^2(C^v)\rangle_z^* = r_g^{*2} = \langle r_g^2(C^v)\rangle/(1 + 2A_2C^vM_w) \quad (2)$$

In the limit $K \to 0$, we have

$$\lim_{K\to 0}\frac{HC^v}{R_c(C^v,0)} = (\partial\pi/\partial C^v)_{T,P}/RT = \frac{1}{M_w} + 2A_2C^v + \ldots \quad (3)$$

where A_2 and M_w are, respectively, the second virial coefficient and the weight-average molecular weight. The symbols T and t are used to denote the absolute temperature and temperature expressed in °C.

Dynamical Properties. The measured single-clipped photocount autocorrelation function for a detector of finite effective photocathode has the form

$$G_k^{(2)}(\tau) = A(1 + b|g^{(1)}(\tau)|^2) \quad (4)$$

where $g^{(1)}(\tau)$ is the normalized correlation function of the scattered electric field, k is the clipping level, A is the background, andd b is an unknown parameter in the data-fitting procedure. τ ($=I\Delta\tau$) is the delay time, with I and $\Delta\tau$ being the delay channel number and the delay time increment, respectively. For a polydisperse sample

$$|g^{(1)}(\tau)| = \int_0^\infty G(\Gamma)\exp(-\Gamma\tau)\,d\Gamma \quad (5)$$

If the polymer coil motion is purely translational in nature, as for the NBS 705 standard polystyrene, where $Kr_g < 1$ in dilute solution, we can analyze the $|g^{(1)}(\tau)|$ function using the cumulants method,[21] with

$$\bar{\Gamma} = \int \Gamma G(\Gamma)\,d\Gamma \quad (6)$$

$$\mu_2 = \int (\Gamma - \bar{\Gamma})^2 G(\Gamma)\,d\Gamma \quad (7)$$

where the variance, $\mu_2/\bar{\Gamma}^2$, is less than 0.1. At higher concentrations, a fast gellike mode is responsible for the anomalous increase in the variance of the line width distribution function $G(\Gamma)$. We then used a histogram method[22] to account for the bimodal behavior in $G(\Gamma)$. It should be noted that the histogram method does not require any a priori assumption on the form of the line width distribution function, but does require approximate $G(\Gamma)$ in terms of step functions. Other methods of approximation for $G(\Gamma)$ should also be feasible. In particular, we may use the methods of splines or discrete multiexponentials. The main purpose of the histogram method is to demonstrate that at higher concentrations, before the overlap concentration C^*, we note a broadening of $G(\Gamma)$, which can be used to explain the increase in the variance, $\mu_2/\bar{\Gamma}^2$, as measured by the cumulants method.

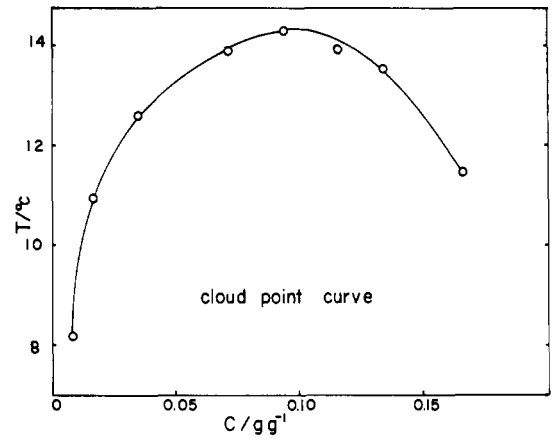

Figure 1. Cloud-point curve of NBS 705 polystyrene in methyl acetate.

In the histogram method

$$|g^{(1)}(\tau)| = \sum_{j=1}^{n} G(\Gamma_j)\int_{\Gamma_j-\Delta\Gamma/2}^{\Gamma_j+\Delta\Gamma/2}\exp(-\Gamma I\Delta\tau)\,d\Gamma \quad (8)$$

where $\sum_{j=1}^{n}G(\Gamma_j)\Delta\Gamma = 1$, with $\Delta\Gamma$ [$=(\Gamma_{max} - \Gamma_{min})/n$] being the width of each step. Values of Γ_{max} and Γ_{min}, signaling the stop and start of the range of the line width distribution function, as well as $G(\Gamma_j)$ are based on minimum deviation between the measured and the calculated time correlation function $G_k^{(2)}(\tau)$. We have used equal steps (or spacings) in our histogram analysis. The effects of histogram step width, in terms of unequal step width or logarithmic step width, on the precision with which we can approximate $G(\Gamma)$ have been examined. Our results are essentially independent of the methods of data analysis. With $\bar{\Gamma} = \bar{D}K^2$, the translational diffusion coefficient for dilute polymer solutions can be expanded to first order in concentration as

$$\bar{D} = \bar{D}_0(1 + k_DC^v + \ldots) \quad (9)$$

At high concentrations, we still have

$$\lim_{K\to 0}\frac{HC^v}{R_c} = (\partial\pi/\partial C^v)_{T,P}/RT \quad (3')$$

and

$$\bar{D} = \frac{C^v}{\bar{f}}(\partial\mu/\partial C^v)_{T,P} \quad (10)$$

where the chemical potential can be related to the osmotic compressibility to yield the frictional coefficient

$$\bar{f} = \frac{M_w(1 - \bar{v}C^v)}{\bar{D}N_A}(\partial\pi/\partial C^v)_{T,P} \quad (11)$$

with $\bar{v}$ being the specific volume of the polymer.

Results and Discussion

Static Properties. Figure 1 shows an experimentally measured cloud-point curve for NBS 705 polystyrene in methyl acetate. It was not done with great precision. It is intended to show that the UCST is about 14 °C. The critical solution concentration, in view of the slight polydispersity (M_w/M_n = 1.07), is located to the right of the

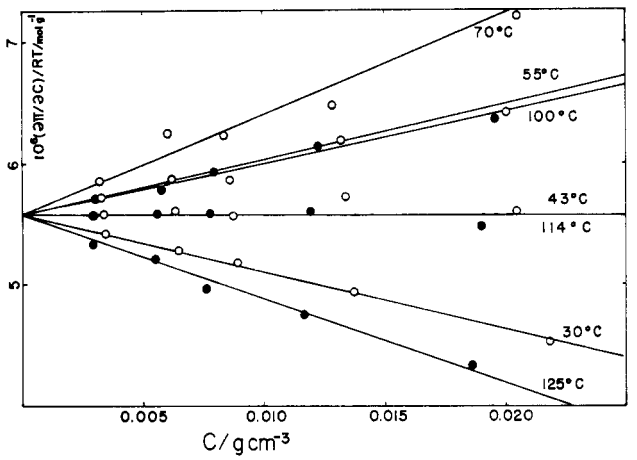

Figure 2. Plots of $(\partial\pi/\partial C)/RT$ vs. concentration at different temperatures in the dilute one-phase region of polystyrene in methyl acetate. Filled circles denote temperatures above 70 °C.

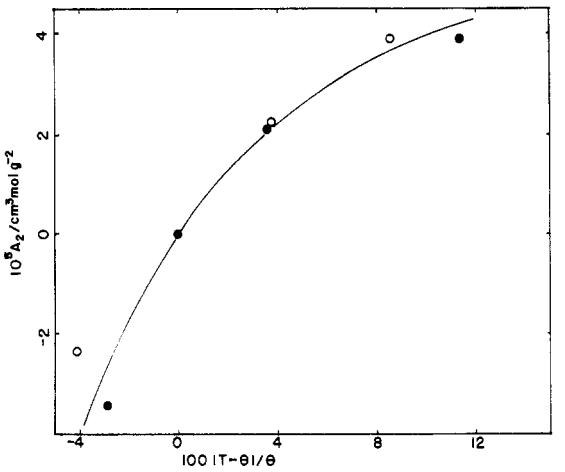

Figure 3. Plot of the second virial coefficient A_2 as a function of reduced temperature distance from upper and lower θ temperatures. Solid circles denote $|T - \Theta_U|/\Theta_U$. Hollow circles denote $|\Theta_L - T|/\Theta_L$, with Θ_U and Θ_L being, respectively, the Flory θ temperature and an assumed lower θ temperature where $A_2 = 0$.

maximum of the cloud-point curve and is in the neighborhood of 10 wt %. Figure 2 shows plots of $(\partial\pi/\partial C^v)/RT$ vs. C^v, where the superscript v has been dropped for convenience. According to eq 3, the intercept is the reciprocal of the weight-average molecular weight while the slope is twice the second virial coefficient A_2. At t = 30 °C, the temperature is below the θ temperature but above the upper critical solution temperature. This is the region where the polymer coil begins to collapse and A_2 is negative. However, as the UCST is still about 16 °C further down and the concentration is less than one-fifth the critical solution concentration, the osmotic compressibility $(\partial\pi/\partial C)_{T,P}$ exhibits negligible critical effects. At t = 43 °C, the system is very near the θ temperature, with $A_2 \approx 0$. As the NBS 705 polystyrene has a fairly low molecular weight of about 1.8×10^5, the temperature distance between the UCST and the Flory θ temperature is quite large, with $\Theta - T_c \sim 43 - 14 \approx 29$ °C.

Consequently, the θ region covers a fairly large temperature range from near the UCST of 14 °C to about (14 + 2 × 29) = 72 °C. In the upper θ region, we should have an increase in A_2 with increasing temperatures. The values of A_2 increase from 0 to 0.24×10^{-4} and 0.39×10^{-4} (cm^3 mol)/g^2 when the temperature increases from 43 °C to 55 and 70 °C, respectively. In Figure 2, we have also noted that $A_2 \approx 0$ at 114 °C. If we *assume* an equivalent spread between the LCST and the lower θ temperature, where $A_2 = 0$, then the LCST has a value of about 143 °C, and the lower θ region covers a temperature range from near 143 °C to about 85 °C. Therefore, the "good" solvent region covering a temperature range of only about 13 °C is virtually nonexistent. The upper and lower θ region shrinks to smaller temperature ranges for higher molecular weight polymers. However, in the present context, it is clear to note that the polystyrene–methyl acetate system has the good solvent region essentially squeezed out by the closeness of the UCST and the LCST. At temperatures higher than 85 °C and in the lower θ region, the second virial coefficient A_2 decreases with increasing temperature, with $A_2 \approx 0$ at 114 °C. The value of A_2 at t = 100 °C with $\Theta_L - T$ = 14 °C is 0.21×10^{-4} (cm^3 mol)/g^2 while $A_2 = 0.22 \times 10^{-4}$ (cm^3 mol)/g^2 at t = 55 °C with $T - \Theta_U$ = 12 °C. Similarly, $A_2 = -0.35 \times 10^{-4}$ (cm^3 mol)/g^2 at t = 125 °C with $T - \Theta_L$ = 11 °C while $A_2 = 0.24 \times 10^{-4}$ cm^3 mol)/g^2 at t = 30 °C with $\Theta_U - T$ = 13 °C. Thus the inversion of the sign for the temperature behavior of A_2 in the upper and lower θ region has clearly been demonstrated by Figure 2. Furthermore, we have noted that all the plots are linear, indicating that eq 3 is obeyed for dilute solutions with the intercepts equivalent to M_w^{-1}. The common intersecting point at zero concentration also illustrates the fact that we were able to perform the experiments at high temperatures to 125 °C without thermal degradation of polystyrene in methyl acetate. In the above discussion, we have noted some symmetry in how A_2 changes with respect to the temperature distance from the θ temperature. Figure 3 shows a plot of the second virial coefficient A_2 vs. the reduced temperature distance from the θ temperature, $|T - \Theta|/\Theta$, with T being the absolute temperature. The subscripts U and L denoting, respectively, the upper and lower θ temperatures have been deleted. However, we have retained the negative sign for those temperatures between the θ temperature and the critical solution temperature. Thus at t = 30 and 125 °C, we have $|T - \Theta|/\Theta$ = 13/(43 + 273) and 11/(114 + 273), or values of 0.041 and 0.028, respectively. At t = 70 °C, we have $|T - \Theta|/\Theta$ = 0.085 and 0.114 for Θ_U and Θ_L, respectively, even though the value of 0.114 using Θ_L is outside the region of unperturbed polymer dimensions based on the lower θ temperature and belongs to the upper θ region. There is an ambiguity in scaling the temperature distance since Θ_U and Θ_L differ by 71 °C. Therefore, we show two points in Figure 3 at $A_2 = 0.39 \times 10^{-4}$ (cm^3 mol)/g^2 at t = 70 °C. Figure 3 shows a slight asymmetry, with the lower θ region exhibiting a larger change in A_2 at 125 °C, or 11 °C above the lower θ temperature (t = 114 °C) when compared with those below the upper θ temperature (t = 43 °C). Nevertheless, the differences are small and the near-symmetrical nature of the temperature–composition diagram in terms of A_2 and $|T - \Theta|/\Theta$ is clearly demonstrated.

The values of A_2 determined from the slope of osmotic compressibility as a function of concentration extrapolated to infinite dilution are listed in Table I. The experimentally determined A_2 were then used to calculate the radius of gyration[16] at each temperature using the modified FKO equation[24-26] as expressed in eq 18 on p 592 of ref 10. We used a measured value of $\langle r_g^2\rangle_z^{1/2}$ = 13.2, 13.6, 13.8, 13.8, 13.7, and 13.4 nm at 30, 55, 70, 100, 114, and 125 °C, respectively. The results again reflect the small differences between upper and lower critical solution temperatures. As the values of $\langle r_g^2\rangle_z$ were quite small, we used the computed values rather than the measured ones in the scaling of concentration in terms of C/C^*, where C^* ($=M_w/(N_A\rho_S\langle r_g^2\rangle_z^{3/2})$, with ρ_S being the solvent density) is the overlap concentration. Figure 4 shows log–log plots of

Table I
Static and Dynamical Properties of NBS 705 Polystyrene (M_w = 179 300, M_w/M_n = 1.07) in Methyl Acetate

	30 °C	43 °C	55 °C	70 °C	100 °C	114 °C	125 °C
$10^7 D_0$, cm²/s	7.50	8.65	9.90	11.80	16.90	19.90	22.80
$10^8 f_0$, g/s	5.58	5.04	4.58	4.01	3.05	2.68	2.41
k_D, cm³/g	−37.10	−30.70	−28.20	−30.60	−33.20	−39.80	−43.10
k_f, cm³/g	27.70	29.80	35.80	43.60	39.80	38.80	29.70
r_h, nm	8.63	8.85	9.00	8.99	8.88	8.75	8.64
r_h/r_g	0.65	0.66	0.66	0.65	0.64	0.64	0.65
r_g, nm	13.20	13.40	13.60	13.80	13.80	13.70	13.40
$10^4 A_2$, (cm³ mol)/g²	−0.235	0	0.22	0.39	0.21	0	−0.35

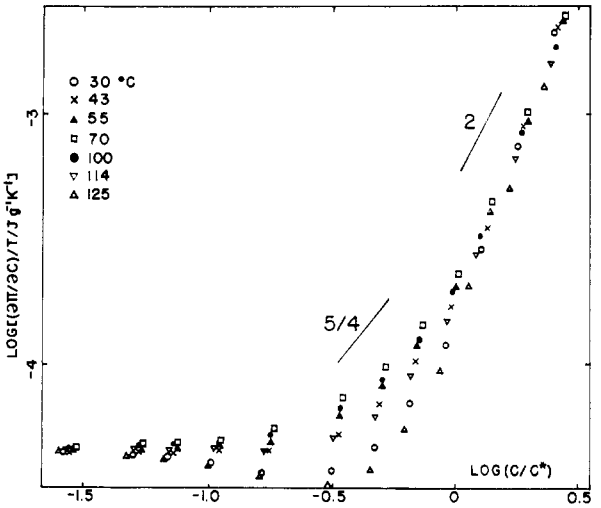

Figure 4. log–log plots of $(\partial\pi/\partial C^v)/T$ vs. C/C^* at different temperatures from dilute to semidilute and concentrated solutions.

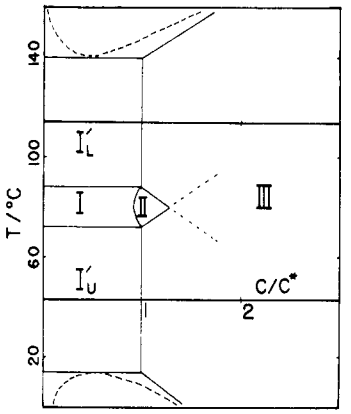

Figure 5. Schematic temperature–concentration diagram for NBS 705 polystyrene in methyl acetate based on results of Figures 1–3 and Table I.

$(\partial\pi/\partial C^v)/T$ vs. C/C^* from 30 to 125 °C, covering temperature ranges from below the Flory Θ temperature to above the lower Θ temperature. The values of $(\partial\pi/\partial C^v)/T$ are almost superimposable in the dilute and concentrated solution regions. For log $(C/C^*) < -1.5$, the points in the log–log plot appear to overlap with one another. Yet we know that log–log plots are notoriously insensitive to small differences. Furthermore, Figure 2 has clearly shown that the slopes (or A_2) change signs from negative at t = 30 °C, zero at t = 43 °C, increasingly positive at t = 55 and 70 °C, decreasingly positive at t = 100 °C, zero at t = 114 °C, and finally negative again at t = 125 °C. However, with the small magnitude of A_2 ($\sim 0.3 \times 10^{-4}$ (cm³ mol)/g²), we can observe only a relatively flat dependence on concentration (or $C^{\sim 0}$) in the log–log plot of $(\partial\pi/\partial C^v)_{T,P}/T$ vs. C/C^* in the dilute solution region. In the semidilute solution region, $(\partial\pi/\partial C^v)_{T,P}/T$ is proportional to $C^{5/4}$. The superposition of data at different temperatures starts to break down as C/C^* approaches 1 from higher concentrations. We have made no attempt to determine the exponent in the semiconcentrated region because methyl acetate is mainly a Θ solvent for polystyrene and the polymer molecular weight is relatively low. Thus we do not know the concentration range over which the value of 2 for the exponent holds. In addition, Figure 4 shows that the curves do not overlap in the transition region where the value of the osmotic compressibility changes gradually. At Θ_U and Θ_L temperatures, as denoted by the crosses (43 °C) and the hollow inverted triangles (114 °C), the two curves do overlap. Similarly, at 55 °C (solid triangles) and 100 °C (solid circles), corresponding to $|T - \Theta|/\Theta = 0.038$ and 0.036, the two curves are very close to each other. In the transition region from dilute to semidilute solutions, the deviation of the curve at 70 °C when compared with those at the Θ temperatures 43 and 114 °C are beyond experimental error limits. Thus the scaling of osmotic compressibility must be modified to adequately predict the solution behavior in the transition region. At temperatures between the Θ temperature and the critical solution temperature, such as those at 30 and 125 °C, the negative value of A_2 in dilute solution can be observed fairly easily. The sharper drop near log $(C/C^*) \sim -0.5$, as shown in Figure 4, can be attributed to the long-range critical effect even though at 30 °C, we are still about 16 °C above the UCST. The larger effect at 125 °C demonstrates that the lower critical solution temperature is perhaps lower than 143 °C, suggesting a more compressed lower Θ region. We determined the phase separation temperature of a 9.3 wt % polystyrene in methyl acetate to be 139.5 °C. Thus LCST is estimated to be 140 °C.

In Figure 5, we have shown schematically a plot of temperature vs. reduced concentration (C/C^*) in the spirit of the phase diagram of Daoud and Jannink.[27] We have used the temperature, instead of the reduced temperature $|T - \Theta|/\Theta$, for the y axis. The dashed curve below 14 °C represents the cloud-point curve. Θ_U and Θ_L are located at 43 and 114 °C, respectively. Regions I_L' and I_U' denote the lower and upper Θ regions where the polymer chain has unperturbed dimensions due to the finite polymer molecular weight. The temperature ranges of I_L' and I_U' shrink with increasing polymer molecular weight. For the NBS 705 polystyrene in methyl acetate, I_U' and I_L' cover most of the one-phase polymer solution region in dilute solution. Region I is *not* a dilute good solvent regime because the excluded volume effects never dominate. It is in a marginal solvent regime and has relatively small values of A_2. Similarly, the radius of gyration never grows very large. Region II, the semidilute region where polymer coils overlap, is hardly accessible. Region III is the dense regime where each polymer coil is in contact with many others.

Dynamical Properties. Results of line width measurements in terms of the z-average diffusion coefficient with $\bar{\Gamma}$ (eq 6) = $\bar{D}K^2$ using the method of cumulants are plotted as a function of concentration at different tem-

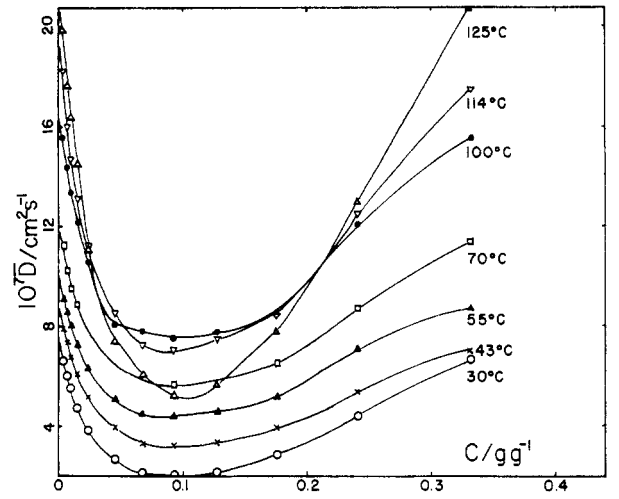

Figure 6. Plots of $\bar{D}$ vs. concentration at different temperatures.

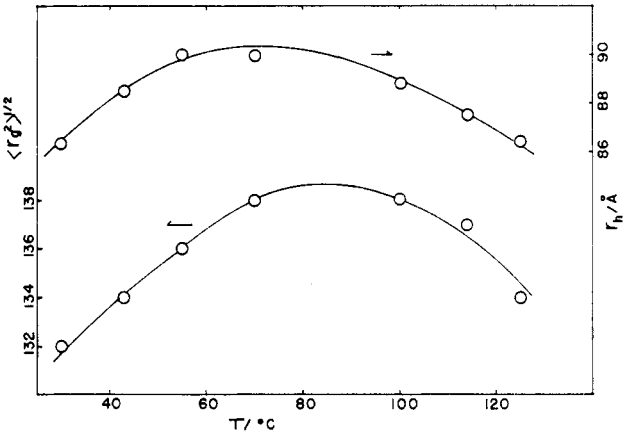

Figure 7. Hydrodynamic radius and radius of gyration of NBS 705 polystyrene in methyl acetate as a function of temperature.

peratures as shown in Figure 6. In the dilute solution regime, eq 9 holds and values of k_D are listed in Table I. All k_D values are negative, indicating a weak thermodynamic ($2A_2M$) term. At higher concentrations, polymer coils begin to overlap and the line width distribution function $G(\Gamma)$ begins to broaden because of increased high-frequency gellike motions. In semiconcentrated solutions, i.e., at concentrations beyond the overlap concentration C^* (>10 wt %), the high-frequency motions begin to dominate. Therefore, at finite concentrations, the average diffusion coefficient, which is a composite of translational and gellike motions, first decreases and then increases with increasing concentration. The minimum occurs near the overlap concentration C^*. It should be noted that the physical meaning of $\bar{D}$ changes as a function of concentration, with translational motion dominating in dilute solution and gellike motion dominating in semidilute and semiconcentrated solutions. The magnitude of $\bar{D}$ should also depend weakly upon scattering angle since the contributions of the two modes in $G(\Gamma)$ at different scattering angles are different. An interesting crossover for the minimum $\bar{D}$ values near and *above* the lower Θ temperature has been observed in Figure 6. The additional decrease in $\bar{D}$ may be attributed to critical slowdown near the LCST. Indeed, if the dramatic effect exists because 125 °C is closer to LCST than 30 °C is to UCST, we have another indication that the lower Θ region is more contracted.

At infinite dilution, we used the Stokes–Einstein relation, $\bar{D}^0 = k_B T/6\pi\eta_0 r_h$, to compute the hydrodynamic radius. The results are listed in Table I. Figure 7 shows plots

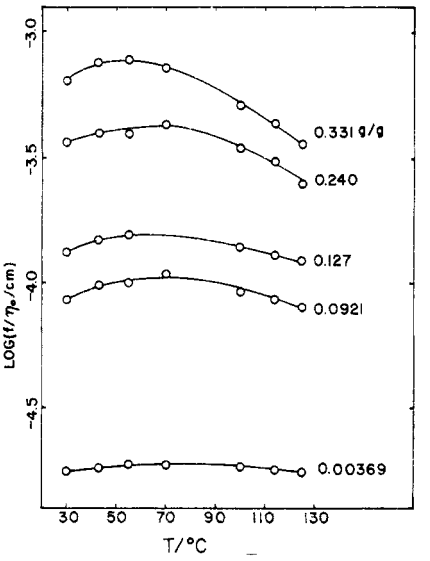

Figure 8. Plots of log (f/η_0) vs. temperature for NBS 705 polystyrene in methyl acetate at different concentrations. η_0 is the solvent viscosity.

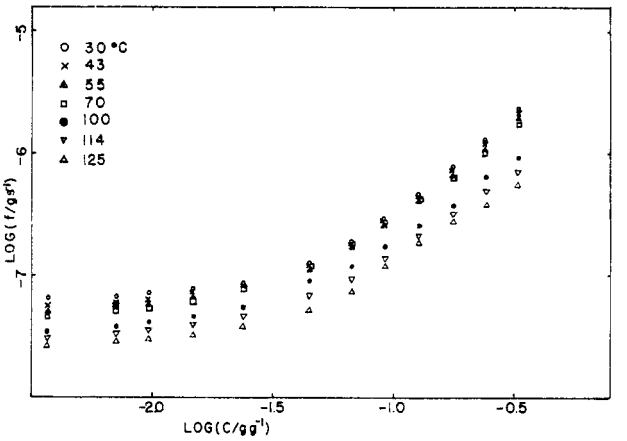

Figure 9. log–log plots of f vs. C for NBS 705 polystyrene in methyl acetate at different temperatures. We have approximated the refractive index increment to be independent of temperature and concentration.

of the hydrodynamic radius and the radius of gyration of NBS 705 polystyrene in methyl acetate as a function of temperature. The ratio of r_h to r_g remains in the neighborhood of 0.65, indicating random coil behavior.

By means of eq 11, we can compute the frictional coefficient f from a combination of intensity $[(\partial\pi/\partial C)_{T,P}]$ and line width ($\bar{D}$) values. In our evaluation, we have taken the refractive index increment to be independent of concentration. This assumption is only approximately correct. We should recall that $\bar{D}$ is a composite diffusion coefficient whose physical meaning changes as a function of concentration. Figure 8 shows plots log (f/η_0) as a function of temperature at different concentrations. The frictional coefficient after correction for the viscosity effect, f/η_0, is essentially independent of temperature in the dilute solution regime, as shown by the relatively flat curve at C = 0.00369 g/g. Thus the different $\bar{D}^0$ values in Figure 6 are mainly due to the changes in solvent viscosity as a function of temperature. The frictional coefficient increases with increasing concentration as shown in Figure 9. The flatness of the curve at C = 0.00369 g/g suggests almost complete overlap of all the curves in Figure 9 if the plots were log (f/η_0) vs. log C as shown in Figure 10, instead of log f vs. log C in the dilute solution region. At higher concentrations, especially those in the semidilute or con-

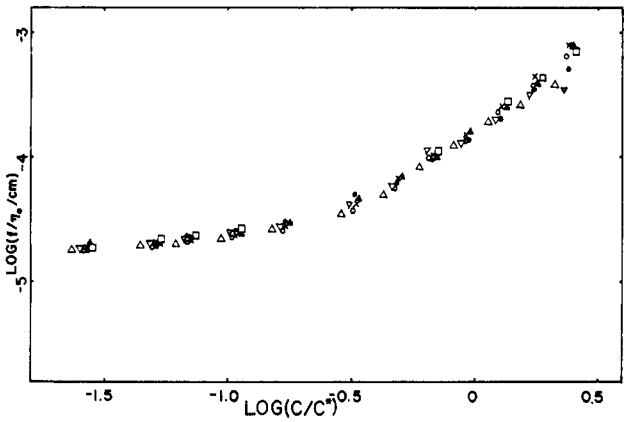

Figure 10. log–log plot of f/η_0 vs. C/C^* for NBS 705 polystyrene in methyl acetate at different temperatures. Appreciable deviation was observed only in the semiconcentrated solution region.

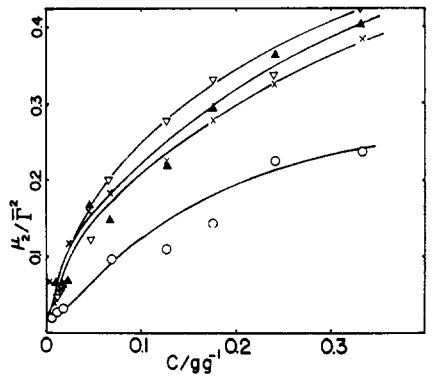

Figure 11. Plots of $\mu_2/\bar{\Gamma}^2$ vs. concentration.

centrated solution region, the maximum in f/η_0 becomes more prominent. In other words, f/η_0 has a positive and then a negative temperature dependence, with the maximum indicating little temperature dependence near region I of Figure 5 and away from I_U' and I_L' in the temperature axis. Figure 9 represents a combination of Figures 4 and 6. With $f \propto (\partial\pi/\partial C)_{T,P}/\bar{D}$, it is interesting to note that the dominating minimum in $\bar{D}$ near the overlap concentration in Figure 6, or the corresponding maximum in a plot of $1/\bar{D}$ vs. C, is absent in Figure 9. The scaling of f/η_0 as a function of C/C^* appears to hold over the entire temperature and concentration range of our studies as shown in Figure 10.

In Rayleigh line width correlation function profile analysis, as we know that the broadening of $G(\Gamma)$ may be attributed to the presence of additional higher frequency motions due to polymer coil overlap at higher concentrations, we need to use other methods of data analysis in addition to the cumulants method. Nevertheless, in a plot of the variance, $\mu_2/\bar{\Gamma}^2$, as a function of concentration, the dramatic increase of its value with increasing concentration even in the dilute solution regime, as shown in Figure 11, demonstrates the existence of additional characteristic times in a system of interacting molecules. The large values of $\mu_2/\bar{\Gamma}^2$ cannot be explained in terms of polydispersity effects. Figures 12 and 13 show the results of our histogram analysis from dilute solution ((a) and (b)) to semiconcentrated solution ((d)) at 30 and 43 °C. In dilute solution, (see (a) and (b)), $G(\Gamma)$ has a relatively narrow and unimodal line width distribution whose variance is essentially related to the molecular weight distribution of the polymer. The average line width $\bar{\Gamma}$ decreases because k_D is negative. Near the overlap concentration, the line width distribution becomes broader, suggesting the existence of additional decay times. Separation of the characteristic

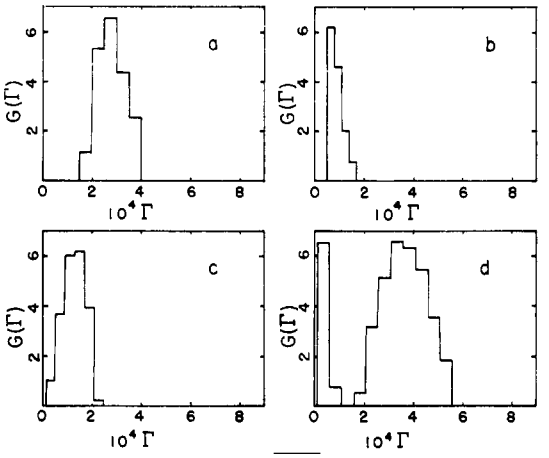

Figure 12. Plots of $G(\Gamma)$ vs. Γ (s^{-1}) for NBS 705 polystyrene in methyl acetate at different concentrations: (a) 0.00369, (b) 0.0920, (c) 0.175, and (d) 0.331 g/g. t = 30 °C, Θ = 75 °C.

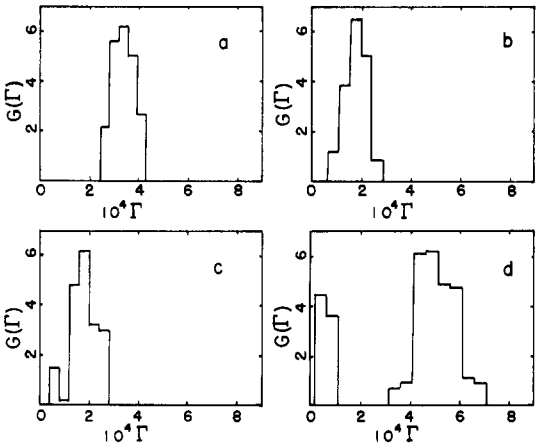

Figure 13. Plots of $G(\Gamma)$ vs. Γ (s^{-1}) for NBS 705 polystyrene in methyl acetate at different concentrations: (a) 0.00369, (b) 0.0920, (c) 0.175, and (d) 0.331 g/g. t = 43 °C, Θ = 75 °C.

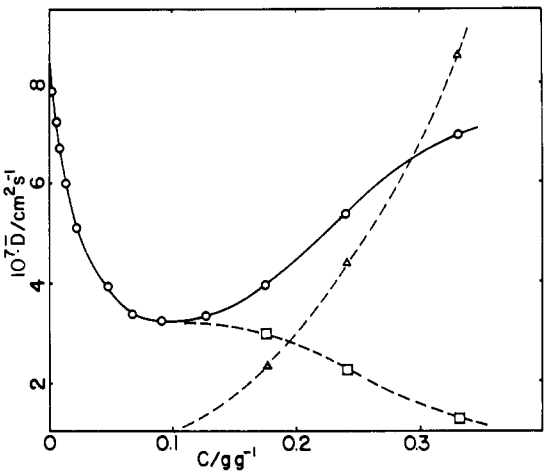

Figure 14. Plots of $\bar{D}$, $\bar{D}_f$, and $\bar{D}_s$ as a function of concentration. The subscripts f and s denote fast and slow modes, respectively.

times, however, remains difficult and arbitrary until we reach very high concentrations (as in (d)), where we clearly see the emergence of a fast gellike mode. The average value of the fast gellike mode increases with increasing concentration, resulting in an increasing $\bar{\Gamma}$ value as shown in Figure 6. Figure 14 shows a more careful decomposition of $\bar{D}$ at 43 °C and Θ = 75 °C. The fast gellike mode appears gradually before the overlap concentration is reached. It increases rapidly with increasing concentration

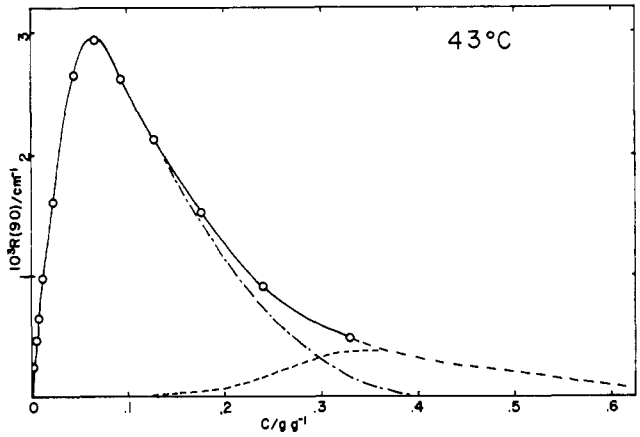

Figure 15. Plot of R_{vv} (θ = 90°) as a function of concentration at 43 °C. Hollow circles denote experimentally measured excess Rayleigh ratio. Dash–dot curve denotes intensity contribution of the slow mode. Dash curve denotes intensity contribution of the fast gellike mode.

while the slower mode, which is related to the translational motion of the polymer coil, slows down and eventually disappears when the solution becomes so concentrated as to essentially form a gel (without permanent cross-links). The magnitude of the intensities contributing to the two modes varies as a function of concentration. Figure 15 shows plots of the excess Rayleigh ratio as a function of concentration. The absolute scattered intensity has been decomposed into two components at $C > 0.1$ g/g using results from the histogram analysis. The behavior of polystyrene in methyl acetate is similar to that of polystyrene in *trans*-Decalin near the upper Θ region.

Acknowledgment. We gratefully acknowledge support of this research by the National Science Foundation, Polymers Program (Grant DMR 8016521).

Registry No. Polystyrene, 9003-53-6.

References and Notes

(1) Edwards, S. F. *Proc. Phys. Soc.* **1966**, *88*, 265. Edwards, S. F.; Jeffers, E. F. *J. Chem. Soc., Faraday Trans. 2* **1979**, *75*, 1020.
(2) de Gennes, P.-G. *Phys. Lett. A* **1972**, *38*, 399. *J. Phys. (Paris)* **1975**, *36*, L-55.
(3) des Cloizeaux, J. *J. Phys. (Paris)* **1975**, *36*, 281.
(4) Kosmas, M. K.; Freed, K. F. *J. Chem. Phys.* **1978**, *69*, 3647. Adler, R. S.; Freed, K. F. *Ibid.* **1979**, *70*, 3119.
(5) Daoud, M.; Cotton, J. P.; Farnoux, B.; Jannink, G.; Sarma, G.; Benoit, H.; Duplessix, R.; Picot, C.; de Gennes, P.-G. *Macromolecules* **1975**, *8*, 804.
(6) Farnoux, B.; Daoud, M.; Decker, D.; Jannink, G.; Ober, R. *J. Phys. (Paris)* **1975**, *36*, L-35.
(7) Cotton, J. P.; Nierlich, M.; Boue, F.; Daoud, M.; Farnoux, B.; Jannink, G.; Duplessix, R.; Picot, C. *J. Chem. Phys.* **1976**, *65*, 1101.
(8) Richards, R. W.; Maconnachie, A.; Allen, G. *Polymer* **1978**, *19*, 266; **1981**, *22*, 147.
(9) Adam, M.; Delsanti, M. *J. Phys. (Paris)* **1976**, *37*, 1045; **1977**, *38*, L-271. *Macromolecules* **1977**, *10*, 1229.
(10) Nose, T.; Chu, B. *Macromolecules* **1979**, *12*, 590, 1122. Chu, B.; Nose, T. *Ibid.* **1979**, *12*, 599; **1980**, *13*, 122.
(11) Schaefer, D. W.; Joanny, J. F.; Pincus, P. *Macromolecules* **1980**, *13*, 1280.
(12) See discussions by: Chu, B. In "Scattering Techniques Applied to Supramolecular and Nonequilibrium Systems" (NATO ASI Series B: Physics); Chen, S.-H., Chu, B., Nossal, R., Eds.; Plenum Press: New York and London, 1980; Vol. 73, pp 231–264.
(13) Delmas, G.; Patterson, D. *Polymer* **1976**, *7*, 513. Patterson, D. *J. Polym. Sci., Part C* **1968**, *16*, 3379. *Pure Appl. Chem.* **1972**, *31*, 133.
(14) Hocker, H.; Shih, H.; Flory, P. J. *Trans. Faraday Soc.* **1971**, *67*, 2275.
(15) For examples, see: Saeki, S.; Kuwahara, N.; Konno, S.; Kaneko, M. *Macromolecules* **1973**, *6*, 246. Kuwahara, N.; Saeki, S.; Konno, S.; Kaneko, M. *Polymer* **1974**, *15*, 66.
(16) Abbey, K. M.; Kubota, K.; Chu, B. In "Scattering Techniques Applied to Supramolecular and Nonequilibrium Systems" (NATO ASI Series B: Physics); Chen, S.-H., Chu, B., Nossal, R., Eds.; Plenum Press: New York and London, 1981; Vol. 73, pp 771–776.
(17) Chu, B.; Kubota, K.; Abbey, K. M. *Polym. Prepr., Am. Chem. Soc., Div. Polym. Chem.* **1981**, *22*, 70.
(18) Richards, R. W.; Maconnachie, A.; Allen, G. *Polymer* **1981**, *22*, 153, 158.
(19) Chen, F. C.; Yeh, A.; Chu, B. *J. Chem. Phys.* **1977**, *66*, 1290.
(20) Tsunashima, Y.; Moro, K.; Chu, B. *Biopolymers* **1978**, *17*, 251.
(21) Koppel, D. W. *J. Chem. Phys.* **1972**, *57*, 4814.
(22) Gulari, Esin; Gulari, Erdogan; Tsunashima, Y.; Chu, B. *J. Chem. Phys.* **1979**, *70*, 3965.
(23) Chu, B.; Gulari, Esin; Gulari, Erdogan *Phys. Scr.* **1979**, *19*, 476.
(24) Kurata, M. "Modern Industrial Chemistry"; Asakura Publishing Co.: Japan, 1975; Vol. 18, p 288.
(25) Imai, S. *Rep. Prog. Polym. Phys. Jpn.* **1965**, *8*, 9.
(26) Yamakawa, H.; Aohi, A.; Tanaka, G. *J. Chem. Phys.* **1966**, *45*, 1938.
(27) Daoud, M.; Jannink, G. *J. Phys. (Paris)* **1976**, *37*, 973.

Structure Determination of the Macromonomer Poly(1,11-dodecadiyne) and Its Cross-Polymerized Product

M. Thakur and Jerome B. Lando*

Department of Macromolecular Science, Case Western Reserve University, Cleveland, Ohio 44106. *Received April 15, 1982*

ABSTRACT: Electron diffraction patterns were obtained from the macromonomer and cross-polymerized crystals of poly(1,11-dodecadiyne). The macromonomer was cast in thin (<200 Å) films from chloroform solution. Cross-polymerization resulted from subsequent exposure of these samples to ^{60}Co γ radiation. Two orientations of the cross-polymerized crystals were obtained by varying the evaporation rate of solvent in the original macromonomer disposition. Thirty-six reflections for the cross-polymerized sample and eighteen reflections for the macromonomer were obtained. Refinement of the structures was accomplished with these data. The unit cell of both macromonomer and cross-polymerized material was monoclinic, space group $P2_1/n$.

Introduction

The cross-polymerization of the macromonomer poly(1,11-dodecadiyne) using UV, X-ray, or ^{60}Co γ radiation has recently been reported.[1] Upon cross-polymerization the sample changes from colorless to dark blue. The term macromonomer is used to describe the original polymer, which has a chemical repeat unit $(-(CH_2)_8-C\equiv C-C\equiv C-)_x$. The term cross-polymerization is utilized to distinguish systematic polymerization of the diacetylene units to a crystalline structure composed of sheets (as indicated in Figure 1) from the more familiar random cross-linking that many polymers undergo when exposed to radiation. The

0024-9297/83/2216-0143$01.50/0